Creating and observing *N*-partite entanglement with atoms

M S Everitt[1], M L Jones[2], B T H Varcoe[2] and J A Dunningham[2]

[1] National Institute of Informatics, 2-1-2 Hitotsubashi, Chiyoda ku, Tokyo 101-8430, Japan
[2] School of Physics and Astronomy, University of Leeds, Leeds LS2 9JT, UK

E-mail: everitt@nii.ac.jp

Abstract
The Mermin inequality provides a criterion for experimentally ruling out local-realistic
descriptions of multiparticle systems. A violation of this inequality means that the particles
must be entangled, but does not, in general, indicate whether *N*-partite entanglement is present.
For this, a stricter bound is required. Here we discuss this bound and use it to propose two
different schemes for demonstrating *N*-partite entanglement with atoms. The first scheme
involves Bose–Einstein condensates trapped in an optical lattice and the second uses Rydberg
atoms in microwave cavities.

(Some figures in this article are in colour only in the electronic version)

1. Introduction

Entanglement is a central feature of quantum mechanics and
the key resource in a wide range of quantum information
processing tasks. Being able to detect and characterize the
entanglement present in a system is therefore an important
challenge for physicists. The first mathematically sharp
method of detecting entanglement for pairs of particles was
proposed by John Bell in 1964 [1, 2]. His now-famous
inequality provided an unambiguous way of distinguishing
quantum–mechanical predictions from those of local-realistic
models. Multiparticle generalizations of the Bell inequality
were subsequently provided by Mermin [3] and others
[4–6]. These can be used to rule out local-realistic models
for *N*-particle systems and are also interesting because there
is a close relationship between their violation and the security
of *N*-partner quantum communications [7].

In general, a violation of these inequalities means that
the particles must be entangled. In fact, by placing a
stricter bound on the inequality [8–10] it is even possible to
determine what class of entanglement is present from
2-entangled to *N*-entangled states. This method has been
used to experimentally confirm three-body entanglement for
photons [11]. In this paper we discuss the conditions required
to demonstrate *N*-partite entanglement and show how it could
be generated and detected in atomic systems. We begin by
reviewing the Mermin inequality and then discuss how it

could be applied to two different atomic systems. In the first,
we consider Bose–Einstein condensates (BECs) trapped in
optical lattices where the two states of each atomic qubit are
different spatial modes. In the second we consider Rydberg
atoms interacting in microwave cavities where the two states
are different electronic levels. For both cases we discuss how
all the terms in the Mermin inequality could be measured
and consider some of the practical issues surrounding
their implementation. In addition this technique may be
suitable for other schemes that produce *N*-partite entanglement
[12–16].

2. Mermin inequality

It is helpful to start with a brief overview of the Mermin
inequality [3]. For this, we consider an *N*-particle GHZ state
of the form

$$|\Phi\rangle_N = \frac{1}{\sqrt{2}}(|\underbrace{\uparrow\uparrow\cdots\uparrow}_{N}\rangle + i|\underbrace{\downarrow\downarrow\cdots\downarrow}_{N}\rangle), \qquad (1)$$

where $\uparrow$ or $\downarrow$ in the jth position labels the two relevant states of
the jth particle. Such a state is known to maximally violate the
Mermin inequality. In an experiment, these *N* particles would
be spatially separated and measurements made on each of

them. Mermin noted that the GHZ state, $|\Phi\rangle_N$, is an eigenstate of the operator

$$A_N = \frac{1}{2i}\left(\prod_{j=1}^{N}\left(\sigma_x^j + i\sigma_y^j\right) - \prod_{j=1}^{N}\left(\sigma_x^j - i\sigma_y^j\right)\right) \quad (2)$$

with eigenvalue 2^{N-1}, where σ_x^j and σ_y^j are respectively the x and y Pauli spin matrices acting on the jth particle. Expanding, $F = \langle\Psi| A_N |\Psi\rangle$, for some general N-particle state $|\Psi\rangle$, one finds

$$F = \langle\Psi| \sigma_y^1\sigma_x^2\cdots\sigma_x^N |\Psi\rangle + \cdots$$
$$- \langle\Psi| \sigma_y^1\sigma_y^2\sigma_y^3\sigma_x^4\cdots\sigma_x^N |\Psi\rangle - \cdots$$
$$+ \langle\Psi| \sigma_y^1\cdots\sigma_y^5\sigma_x^6\cdots\sigma_x^N |\Psi\rangle + \cdots - \cdots, \quad (3)$$

where each line of (3) contains all distinct permutations of the operators in the term shown on that line. The only non-zero terms contain odd numbers of σ_y operators. For the GHZ state, we have $F = {}_N\langle\Phi| A_N |\Phi\rangle_N = 2^{N-1}$.

The corresponding value of F for a local hidden-variable state can be found as follows. Following Mermin, we consider the case where the measured distribution functions, $P_{\mu_1\cdots\mu_N}(m_1\cdots m_N)$, where $\mu_j \in \{x, y\}$ and $m_j \in \{\uparrow, \downarrow\}$, that describe the 2^{N-1} measurements that must be performed to yield the correlations in (3), can be written in the conditionally independent form

$$P_{\mu_1\cdots\mu_N}(m_1\cdots m_N)$$
$$= \int d\lambda \rho(\lambda)\left[p_{\mu_1}^1(m_1, \lambda)\cdots p_{\mu_N}^N(m_N, \lambda)\right] \quad (4)$$

where $p_{\mu_i}^i(m_i, \lambda)$ is the probability distribution of results for a measurement in the μ_i basis on particle i. This general hidden-variable form attributes the correlations to some unspecified set of parameters, λ, common to all N particles, with distribution $\rho(\lambda)$. It accounts for correlations in terms of information jointly available to the particles when they left their common source. Mermin showed that such a local hidden-variable state has the bounds [3]

$$\begin{aligned} F &\leqslant 2^{N/2}, & N \text{ even},\\ F &\leqslant 2^{(N-1)/2}, & N \text{ odd}. \end{aligned} \quad (5)$$

We see that the GHZ state, $|\Phi\rangle_N$, for which $F = 2^{N-1}$, violates (5) by an exponential amount.

A violation of inequality (5) demonstrates that the particles are entangled, but does not guarantee N-partite entanglement [17]. For this, a tighter bound is needed, which can be found as follows. We assume that there is, at most, $(N - 1)$-partite entanglement in the system. This means that the state of one of the lattice sites (say the first one) factorizes and the expectation value of the corresponding operator factorizes in each term in (3). Then using the fact that all expectation values disappear if they contain an even number of σ_y operators, it is straightforward to show that we are left with

$$F = \langle\sigma_x\rangle F_{N-1} \leqslant 2^{N-2}, \quad (6)$$

where the last step follows because $\langle\sigma_x\rangle \leqslant 1$ and $F_{N-1} = 2^{N-2}$. This agrees with the condition found for three particles in [9]. Any state that violates (6) must have at least N-partite entanglement.
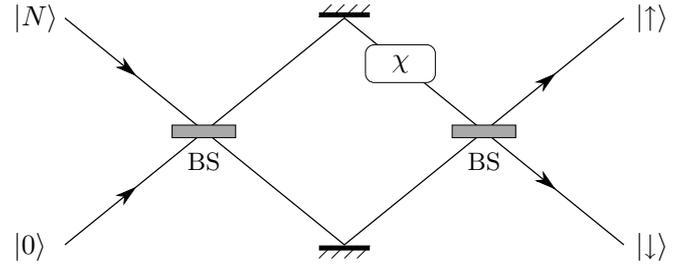
Figure 1. Schematic diagram of the GHZ state creation procedure. The scheme takes the form of a Mach–Zehnder interferometer consisting of two 50:50 beam splitters (BS), but with the addition of a nonlinearity, χ, on the upper path. If N particles are fed into one input port and the nonlinearity is applied for time $t = \pi/(2\chi)$, the output is the GHZ state given by (1).

3. Implementation with BECs

The aim of an experiment would be to measure all the expectation values in (3) and see firstly whether their sum violates the bound given by (5), in which case entanglement is present, and secondly whether it violates the bound given by (6) in which case N-partite entanglement is present. We now discuss how such a scheme could be implemented with BECs.

The first step is to create a GHZ state of the form (1). Various proposals have been made for producing such states in the laboratory [18–21]. Experiments have successfully created GHZ states with small numbers of photons [22, 23] and ^{9}Be$^+$ ions [13, 16, 24], and could in principle be scaled up to larger numbers. Here we consider the case of BECs where states of the form (1) can be created using beam splitters and nonlinear unitary evolution [25]. For BECs, the nonlinearity arises naturally as a result of collisions between the atoms.

A detailed study of the state preparation scheme is presented elsewhere [25], but essentially consists of a Mach–Zehnder interferometer with nonlinear evolution between the two beam splitters (see figure 1). The input state consists of N particles at one port and none at the other. If the nonlinearity is applied only to the upper path of the interferometer, the nonlinear part of the Hamiltonian has the form $H_{nl} = \chi \hat{n}_\uparrow(\hat{n}_\uparrow - 1)$, where $\hat{n}_\uparrow$ is the number operator for the upper path and χ is the strength of the nonlinearity. Evolution due to this Hamiltonian for time $t = \pi/(2\chi)$ then gives state (1) at the output.

Experimentally, this state creation for BECs would involve loading a BEC into one trap of a double-well potential. For now, we consider that the BEC is in a Fock state with N atoms, i.e. $|N\rangle$; however, later we will consider the case of a mixed state. The first beam splitter is implemented simply by rapidly reducing the height of the potential barrier between the two wells, waiting for time $t = \pi/(4J)$, where J is the strength of the tunnelling between the wells, and then rapidly raising the barriers again [26]. The nonlinearity can then be 'switched on' for time $t = \pi/(2\chi)$ by the use of Feshbach resonances to change the interaction strength, χ, between the atoms [27]. Finally another beam splitter can be implemented. This gives a state of the form (1), where the labels $\uparrow$ and $\downarrow$
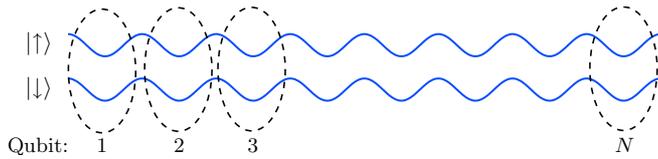
Figure 2. The two spatially separated optical lattices. Each pair of lattice sites (marked by a dashed curve) represents a qubit and contains a single atom. An atom in the upper trap is denoted $|\uparrow\rangle$ and an atom in the lower trap is denoted $|\downarrow\rangle$.

refer to the two potential wells, shown as the upper and lower outputs from the interferometer in figure 1.

After the state creation process, we have a superposition of all the atoms in the upper trap and the lower trap. The two traps are then illuminated with a retro-reflected laser field that creates a standing wave across them both (see figure 2). The frequency of this laser is chosen so that the atoms are trapped in the nodes of the standing wave. By adiabatically increasing the intensity of the light, the number fluctuations on each site are progressively squeezed due to the interplay between the interaction and tunnelling energies. Eventually, a Mott insulator transition [28] takes place whereby each pair of upper and lower lattice sites contains precisely one atom. Each qubit in (1) is now spatially distinct, and we take ↑ to represent an atom in the upper lattice site and ↓ to represent one in the lower lattice site.

The next step is to make measurements on this system that correspond to the terms in (3). This involves making measurements on each qubit in the basis of the eigenstates of σ_x and σ_y. The eigenstates of σ_x are $|x, +\rangle = (|\uparrow\rangle + |\downarrow\rangle)/\sqrt{2}$ and $|x, -\rangle = (|\uparrow\rangle - |\downarrow\rangle)/\sqrt{2}$ with eigenvalues of +1 and −1 respectively. The eigenstates of σ_y are $|y, +\rangle = (|\uparrow\rangle + i|\downarrow\rangle)/\sqrt{2}$ and $|y, -\rangle = (|\uparrow\rangle - i|\downarrow\rangle)/\sqrt{2}$ with eigenvalues of +1 and −1 respectively.

These measurements can be achieved by passing the two sites of each qubit through a beam splitter. We can see this as follows. The transformation of the single-particle states by a 50:50 beam splitter is

$$|\uparrow\rangle \longrightarrow \tfrac{1}{\sqrt{2}} \left(|\uparrow\rangle + i|\downarrow\rangle\right) \qquad (7)$$

$$|\downarrow\rangle \longrightarrow \tfrac{1}{\sqrt{2}} \left(i|\uparrow\rangle + |\downarrow\rangle\right). \qquad (8)$$

Using this, it is straightforward to show that if we pass the eigenstates of σ_y through a 50:50 beam splitter, we obtain $|y, +\rangle \to |\uparrow\rangle$ and $|y, -\rangle \to |\downarrow\rangle$, where we have ignored any irrelevant global phase. This means that using a beam splitter and then detecting whether the particle is in the upper or lower site is equivalent to a measurement in the σ_y basis. A detection result of $|\uparrow\rangle$ or $|\downarrow\rangle$ gives a measurement outcome in the σ_y basis of +1 or −1 respectively.

For measurements in the σ_x basis, we need a combination of a phase shift and a beam splitter. We can see this by considering the eigenstates of σ_x. The combined procedure of applying a phase shift of $\pi/2$ to the upper site and then passing the state through a 50:50 beam splitter transforms the states in the following way: $|x, +\rangle \to |\uparrow\rangle$ and $|x, -\rangle \to |\downarrow\rangle$. A detection result of $|\uparrow\rangle$ or $|\downarrow\rangle$ is therefore equivalent to a measurement outcome in the σ_x basis of +1 or −1 respectively.

In practice, to measure one of the terms in (3), we would imprint a phase shift on all the sites for which we want to make a σ_x measurement. The procedure for doing this is well understood and has been experimentally demonstrated [29]. It involves illuminating the target lattice sites with pulsed off-resonant laser light. The phase that is imparted is a function of the detuning of the laser, the laser linewidth, the intensity of the light, and the pulse duration. An appropriate choice of these parameters allows a $\pi/2$ phase to be imprinted. Next we would simultaneously implement a 50:50 beam splitter between each upper site and its corresponding lower site. This can be achieved simply by rapidly lowering the potential barrier between the upper and lower lattices, waiting for some time $t = \pi/(4J)$ and then rapidly raising the barriers again [26]. The measurement outcome depends on the number of atoms in the lower, $N_\downarrow$, and upper, $N_\uparrow$, traps and is given by

$$(-1)^{N_\downarrow}(+1)^{N_\uparrow} = (-1)^{N_\downarrow}. \qquad (9)$$

So, in fact, we need only measure the number of atoms in the lower traps. To find the corresponding term in (3), we need an ensemble average of these measurements and the whole procedure then needs to be repeated for all the terms in (3). This would allow one to experimentally determine a value for F and see whether it violates the bounds given by (5) and (6).

Of course, this all depends on how accurately we are able to measure $N_\downarrow$. This will be affected by two main processes: the efficiency of our number counting detectors and any imperfections in the beam splitting operation that is used to transform the state into the eigenbases of the σ_x and σ_y operators. The combination of these two effects will lead to an overall detection efficiency, $\eta < 1$. A straightforward calculation shows that in order to confirm N-partite entanglement, we require

$$\eta \geqslant 1 - \frac{1}{4N}. \qquad (10)$$

A similar scaling for the detector efficiencies required to detect macroscopic superposition states has previously been identified in other work [30]. From (10), we see that the deviations of the detector efficiencies from unity and the deviations of the beam splitter reflectivities from 50% must scale as $1/N$. This means that this scheme is likely to only be practical for small numbers of atoms. However, if we are only interested in confirming that there is entanglement present (rather than N-partite entanglement), the condition on η becomes much less stringent. In this case we have

$$\eta \geqslant \sqrt{2^{-(1+1/N)}} \approx 1/\sqrt{2}, \qquad (11)$$

which should be achievable in experiments. A nice feature of this is that the condition depends only very weakly on N.

One possible difficulty with this scheme is that it requires the experimenter to be able to individually address lattice sites. This is difficult because the lattice sites are spaced by $\lambda/2$, where λ is the wavelength of the laser light, and so they are too close to easily resolve. There are, however, a number of suggestions for how this problem may be able to be overcome. In one experiment, atoms were loaded into every third lattice site by superimposing a 'superlattice' on top of the regular lattice [31]. Another idea is to change the spacing between lattice sites by controlling the angle at which the laser beams

interfere [32]. In such a setup one could quickly separate the atoms so that they can be addressed individually to imprint phases or make measurements. A recent experiment has also shown how it is possible to resolve single atoms in a Mott insulator state using fluorescence imaging [33].

Other practical issues with implementing this scheme are decoherence as well as other imperfections in the GHZ state creation process. It has been shown elsewhere [25] that it is possible to create good approximations to GHZ states using the scheme described above even when there is loss present during the preparation. Because the final state will not be a perfect GHZ state, maximal violation of the Mermin inequality (i.e. $F = 2^{N-1}$) will not be observed. However significant violations should still be able to be measured. The degree of violation would be a useful diagnostic of the state and how good the state preparation scheme is. Decoherence after the GHZ state has been created is fundamental and unavoidable. As with all such schemes, this will limit the size of the entangled state that can be created and measured. However, the scheme presented here provides a convenient way of analysing this decoherence process. By measuring the value of F for the GHZ state after different times, the timescale of decoherence could be determined since the violation of the inequality will decrease as loss destroys the entanglement present. A similar idea was experimentally realized with mesoscopic superpositions of different microwave coherent states [34].

So far, we have considered the case that the total number of atoms, N, is fixed and known. However, in practice, the input BEC will be a mixture of number states and so each experimental run will correspond to a different total number of atoms. This means that the expectation values corresponding to each term in the expansion (3) will be averages over different particle numbers. We now show how it is possible to extract the relevant data to use in equation (3) even though the particle number is different in each trial.

We suppose that for N atoms in the final state, a single atom populates each of the first N sites on the optical lattice in the Mott regime[3]. In our scheme, we will consider only the first $N_{\min}$ sites, where $N_{\min}$ is the minimum number of atoms on any run. Importantly, we retain only experimental runs for which all the σ_y measurements take place in the first $N_{\min}$ sites (see figure 3). This gives us a subset of $2^{N_{\min}-1}$ measurements from all those taken and we neglect the rest. In order for this approach to work, we need to show that all the expectation values in (3) for $N_{\min}$ are identical to the results obtained if, for $N > N_{\min}$, we measure only a subset consisting of the first $N_{\min}$ sites. We can confirm this by calculating the expectation values directly.

For N atoms, the expectation value for a general term in (3), where all the σ_y measurements are in the first $N_{\min}$ sites, has the form

$$_N \langle \Phi | \overbrace{\sigma_y^1 \cdots \sigma_y^j \sigma_x^{j+1} \cdots \sigma_x^{N_{\min}}}^{\text{First } N_{\min} \text{ sites}} \sigma_x^{N_{\min}+1} \cdots \sigma_x^N | \Phi \rangle_N = -\mathrm{i}^{j+1},$$ (12)

---

[3] We take the first N sites for notational simplicity. We could, of course, also consider that the atoms populate the N middle sites of the lattice with a trivial extension to the algebra.
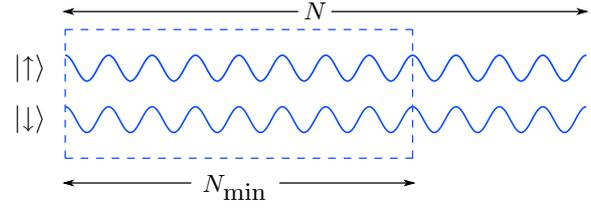
Figure 3. The two optical lattices. In the Mott regime, we assume that for N atoms, each of the first N pairs of upper and lower lattice sites contains a single atom. To account for fluctuations in the total atom number between experimental runs, we consider only the cases where all σ_y measurements take place in the first $N_{\min}$ sites, where $N_{\min}$ is the minimum total number of atoms on any experimental run.

where the last step follows because we only have terms where j is odd. Any permutation of the first $N_{\min}$ operators does not change the result.

Similarly, for $N_{\min}$ atoms, we obtain

$$_{N_{\min}} \langle \Phi | \sigma_y^1 \cdots \sigma_y^j \sigma_x^{j+1} \cdots \sigma_x^{N_{\min}} | \Phi \rangle_{N_{\min}} = -\mathrm{i}^{j+1}.$$ (13)

Comparing (12) and (13), we see that by making measurements on $| \Phi \rangle_N$, we can determine the corresponding expectation values for $| \Phi \rangle_{N_{\min}}$. This means that, even when the total number of atoms varies between experimental runs, we can always obtain a complete set of $2^{N_{\min}-1}$ terms corresponding to the expansion in (3) where $N = N_{\min}$. In this way, the value of this expression for a GHZ state is $F = 2^{N_{\min}-1}$, and the bound for $(N_{\min} - 1)$-partite entanglement is

$$F \leqslant 2^{N_{\min}-2}.$$ (14)

The corresponding bound for the hidden-variable model follows easily from (4) since the joint probability for N sites can be reduced to a joint probability for $N_{\min}$ sites simply by integrating over $m_{N_{\min}+1}, \cdots, m_N$. This gives

$$P_{\mu_1 \cdots \mu_{N_{\min}}}(m_1 \cdots m_{N_{\min}})$$
$$= \int \mathrm{d}\lambda \rho(\lambda) \left[p_{\mu_1}^1(m_1, \lambda) \cdots p_{\mu_N}^N(m_{N_{\min}}, \lambda) \right],$$ (15)

i.e. the first $N_{\min}$ sites do not depend on the measurement outcomes of the last $N - N_{\min}$ sites. The rest of the argument follows that of Mermin [3] but with N replaced with $N_{\min}$. This gives the hidden-variable bounds as

$$\begin{aligned} F &\leqslant 2^{N_{\min}/2}, & N_{\min} \text{ even}, \\ F &\leqslant 2^{(N_{\min}-1)/2}, & N_{\min} \text{ odd}. \end{aligned}$$ (16)

Comparing (16) and (14) with the result for a GHZ state, $F = 2^{N_{\min}-1}$, we see that it is still possible to detect $N_{\min}$-partite entanglements even if the total number of atoms in the system is uncertain.

4. Implementation with cavity QED

Another possible system for implementing this scheme that is likely to be more accessible to experiments is Rydberg atoms in microwave cavities. For this, we consider an N-particle GHZ state of the form

$$| \Phi \rangle_N = \tfrac{1}{\sqrt{2}} \big(| \underbrace{gg \cdots g}_{N} \rangle + | \underbrace{ee \cdots e}_{N} \rangle \big),$$ (17)

where g or e in the jth position denotes that the jth particle is in the ground or excited state. This state and the subsequent analysis differ slightly from that discussed in the first part of the paper. We choose to do the analysis for this particular state because it is the one most conveniently created by our proposed experimental scheme for Rydberg atoms.

This GHZ state, $|\Phi\rangle_N$, is an eigenstate of the operator

$$A_N = \frac{1}{2}\left(\prod_{j=1}^{N}(\sigma_x^j + \mathrm{i}\sigma_y^j) + \prod_{j=1}^{N}(\sigma_x^j - \mathrm{i}\sigma_y^j)\right) \qquad (18)$$

with eigenvalue 2^{N-1}. For a general N-particle state $|\Psi\rangle$, one finds $F = \langle\Psi|A_N|\Psi\rangle$ which is given by

$$F = 1 - \langle\Psi|\sigma_y^1\sigma_y^2\sigma_x^3\sigma_x^4\cdots\sigma_x^N|\Psi\rangle - \cdots$$
$$+ \langle\Psi|\sigma_y^1\cdots\sigma_y^4\sigma_x^5\cdots\sigma_x^N|\Psi\rangle + \cdots$$
$$- \langle\Psi|\sigma_y^1\cdots\sigma_y^6\sigma_x^7\cdots\sigma_x^N|\Psi\rangle - \cdots + \cdots. \qquad (19)$$

For the GHZ state (17), we have $F = {}_N\langle\Phi|A_N|\Phi\rangle_N = 2^{N-1}$, and any hidden-variable state has the same bounds as before, i.e.

$$\begin{aligned} F &\leqslant 2^{N/2}, & N \text{ even}, \\ F &\leqslant 2^{(N-1)/2}, & N \text{ odd}. \end{aligned} \qquad (20)$$

The first step to seeking violations of (20) using Rydberg atoms is to create a GHZ of the form (17). We start with N atoms of ^{85}Rb, each initially in the Rydberg state 63P. Using resonant microwave fields, transitions can be driven to the levels 61D and 62P. We shall refer to 63P as $|e\rangle$, the relative excited state, and 61D as $|g\rangle$, the relative ground state. These form the basis used to construct the GHZ state. The state 62P is referred to as $|i\rangle$, an auxiliary state. The state $|e\rangle$ is produced using a three-step laser excitation [35]. Zheng and Guo demonstrate in their paper [36] that by using three states in this manner with a cavity detuned from the $|e\rangle \leftrightarrow |g\rangle$ transition, it is possible to create an EPR state with a pair of atoms. This was later demonstrated experimentally by Osnaghi *et al* [37]. We extend this scheme to show that by using the same states and $N-1$ cavities in a line, it is possible to produce a GHZ state of N atoms[4]. An alternative has been demonstrated by Rauschenbeutel *et al* [12].

We start with all atoms initially in the state $|e\rangle$. These atoms are produced on demand [38]. Next all atoms are rotated to the state $|+\rangle = (|g\rangle + |e\rangle)/\sqrt{2}$ using a microwave field resonant with the $|e\rangle \leftrightarrow |g\rangle$ transition; see figure 4. This corresponds to a rotation about the x-axis on the Bloch sphere. The Hamiltonian used to implement this is

$$H_I = \hbar\Omega(\hat{\sigma}^+ + \hat{\sigma}^-), \qquad (21)$$

where Ω is the coupling strength of the atom with the field and $\hat{\sigma}^+$ and $\hat{\sigma}^-$ are the atomic raising and lowering operators. The amplitudes of the atom given as $a(t)|g\rangle + b(t)|e\rangle$ evolve according to the equations

$$\begin{aligned} a(t) &= a_0\cos(\Omega t) - \mathrm{i}b_0\sin(\Omega t) \\ b(t) &= b_0\cos(\Omega t) - \mathrm{i}a_0\sin(\Omega t), \end{aligned} \qquad (22)$$

which is equivalent to a rotation about the x-axis.

[4] Alternatively we could use atoms at different velocities and a single cavity so that one atom is present during the passage of the other atoms, which are only present one at a time, effectively emulating multiple cavities.
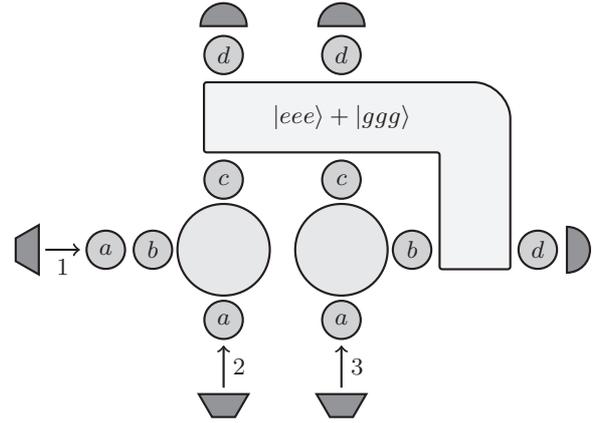
Figure 4. This example produces a three-party GHZ state of atoms. Atoms approach as indicated by arrows to coincide in each cavity (large circles). Initially all atoms are in the state $|e\rangle$. The rotation zones labelled a take $|e\rangle$ to $|+\rangle$ and c take $|e\rangle$ to $|-\rangle$ and $|g\rangle$ to $|+\rangle$. Those zones labelled b act on the first atom (travelling horizontally) to switch $|e\rangle$ components of the state to $|i\rangle$, the auxiliary state, and vice versa. The enclosed region is where the GHZ state exists. The zones labelled d are arbitrary rotations used to study the state before measurement.

The first atom, which will interact with each other atom in turn, then passes through another microwave field (labelled as b in figure 4) which is resonant with the transition $|e\rangle \leftrightarrow |i\rangle$ leaving the first atom in the state $(|g\rangle + |i\rangle)/\sqrt{2}$. The first atom now interacts with the second in a high-Q (quality factor) microwave cavity. This cavity is detuned from the $|e\rangle \leftrightarrow |g\rangle$ resonance. The four possible states that may interact are shown in the left column of table 1. The first two states in the left column of the table are modelled using a two-atom Tavis–Cummings model with large detuning. With a zero photon field [39] this can be solved to give the interaction

$$\begin{aligned} |g, e\rangle &\mapsto \mathrm{e}^{-\mathrm{i}\gamma t}[\cos(\gamma t)|g, e\rangle - \mathrm{i}\sin(\gamma t)|e, g\rangle] \\ |g, g\rangle &\mapsto |g, g\rangle \end{aligned} \qquad (23)$$

where $\gamma = g^2/\Delta$, g is the atom–field coupling constant and Δ is the detuning. As the field is detuned from the transition, excited atoms can only virtually excite the field, effectively coupling the atoms together and allowing an excitation to be passed between atoms. The zero photon stipulation is satisfied in the laboratory by cryogenically cooling the cavity, and possibly by preceding the experiment with a chain of atoms in the state $|g\rangle$ to unload the field. The second two states in the left column of table 1 each have one atom in the state $|i\rangle$, for which all transitions are so far from the cavity resonance that we may assume that it does not contribute to the dynamics of the system. This leaves one atom and the detuned field, which is modelled using the Jaynes–Cummings model. In the case of zero photons and large detuning the evolution of these two states is given by

$$\begin{aligned} |i, e\rangle &\mapsto \mathrm{e}^{-\mathrm{i}\gamma t}|i, e\rangle \\ |i, g\rangle &\mapsto |i, g\rangle. \end{aligned} \qquad (24)$$

For creating a GHZ state we choose the interaction time and detuning such that $t = \pi/4\gamma$. For each interaction this provides the right-hand side of the truth table 1.

Table 1. The collisional phase gate. The truth table for the collisional phase gate introduced in [36].

Input	Output
$|g, g\rangle$	$|g, g\rangle$
$|g, e\rangle$	$|g, e\rangle$
$|i, g\rangle$	$|i, g\rangle$
$|i, e\rangle$	$-|i, e\rangle$

After the interaction with the first atom, each atom emerging from each cavity is rotated so that $|g\rangle \to |+\rangle$ and $|e\rangle \to |-\rangle = (|g\rangle - |e\rangle)/\sqrt{2}$. After the first atom emerges from the final cavity, it enters a microwave field that drives the transition $|i\rangle \leftrightarrow |e\rangle$ so that the atom is left with no amplitude in $|i\rangle$. The atoms are now in a GHZ state ready for use. Figure 4 demonstrates the construction of a three-atom GHZ state. It is also possible to generate larger entangled structures with more elaborate cavity arrays [40].

Now we need to make measurements on this system that correspond to the terms in (19). This involves making measurements on each qubit in the basis of the eigenstates of σ_x and σ_y, i.e. $|g\rangle \pm |e\rangle$ and $|g\rangle \pm i|e\rangle$ respectively. The rotations take place in the regions labelled d in figure 4. The rotation in the basis of σ_x has already been discussed, and only one other rotation on the Bloch sphere is needed to realize a rotation in the basis of σ_y.

The second operation we use is a rotation about the z-axis of the Bloch sphere, R_z. This can be implemented simply by applying an electric field to the atom. This effectively increases the transition energy between the levels of the atom and results in a modified phase evolution for the two states. This technique has been experimentally demonstrated with sodium Rydberg atoms by Ryabtsev *et al* [41]. They applied a resonant microwave pulse to perform an x-rotation between two sodium Rydberg atoms followed by a Stark shift z-rotation and another x-rotation. This combination of interactions allowed them to perform Ramsey interferometry of the R_z operation applied by the Stark shift. Their results confirmed that they had successfully implemented the phase operation R_z and that it was coherent [41].

For Rydberg states of alkali metals, the Stark shift varies approximately quadratically with the electric field strength [42]

$$\delta_{g,e} \propto -\alpha_{g,e} E^2, \qquad (25)$$

where $\alpha_{g,e}$ is the polarizability of the ground or excited state of the atom and E is the amplitude of the electric field. The polarizability of the two states will be different, so the relative phase shift will be given by

$$\Theta = \epsilon(\alpha_g - \alpha_e)E^2, \qquad (26)$$

where ϵ is a factor calculated by integrating over the pulse shape of the electric field. Applying the electric field for some time t, the state of the atom evolves as

$$a|e\rangle + b|g\rangle \mapsto e^{-i\Theta t} a|e\rangle + b|g\rangle. \qquad (27)$$

This corresponds to a rotation about the z-axis, where Θt is the angle of rotation.

Now, in order to measure an atom in the σ_x basis, we simply apply the resonant microwave field to implement a rotation of the state by $\pi/2$ about the y-axis and then measure the atom to see whether it is in the state $|g\rangle$ or $|e\rangle$. We can see that this works because the rotation maps the eigenstates of σ_x directly onto the states $|g\rangle$ and $|e\rangle$. Similarly, to measure in the σ_y basis we apply a $\pi/2$ rotation about the z-axis (using the Stark shift), then a $\pi/2$ rotation about the y-axis, and then measure the atom to see whether it is in $|g\rangle$ or $|e\rangle$. Measuring Rydberg atoms is discussed by Gallagher [43]. The particular measurement process that is useful in this experiment, state selective field ionization, is described in [39].

This scheme will suffer from similar practical limitations as those outlined above for the BEC scheme. In particular, decoherence, vibrations, and imperfect rotations in Bloch space will lead to an imperfect GHZ state being created. Such considerations will limit this scheme to small numbers of atoms. However, it should still be possible to detect violations of the Mermin inequality. In their paper, outlining the controlled phase gate that we employ here [36], Zheng and Guo note the effect of errors in the time of arrival of one of the atoms. They found that for a particular interaction time t for which ideally an EPR pair is produced, one atom entering the cavity $0.01t$ before the other produced a fidelity of $|\langle\psi_{EPR}|\psi\rangle|^2 \approx 0.99$. We expect that with appropriate single atom sources much smaller errors in arrival time will be achievable. Vibrational shifts in the frequency of the cavity should also be considered. As the interaction is off resonant with the cavity, this will induce small shifts in the interaction strength. Assuming that for a good interaction $\Delta = 10\,g$, where g is the atom–cavity coupling constant, then the effective atom–atom coupling constant is $\gamma = g/10$. For a micromaser such as that reported in [39] a g on the order of 10 kHz is typical. A pessimistic estimate of a shift in the cavity frequency on the order of 1 kHz leads to a shift in the effective coupling constant of approximately 1%. For up to a ten-atom GHZ state this leads to a fidelity of $|\langle\psi_{EPR}|\psi\rangle|^2 \approx 0.99$. From this we conclude that the greater difficulty is producing atoms on demand and targeting them precisely to encounter the same cavity field profile. Transient misalignment induced by vibrations will be particular to the apparatus used, and this must be determined experimentally.

Finally we ought to comment on how noise affects these results since it is well known that detector inefficiencies in particular give rise to the so-called detection loophole which can undermine our ability to exclude local-realistic descriptions using Bell-type inequalities. Braunstein and Mann [44] have considered this problem and shown that if the noise is sufficiently small, then the signal for violation grows exponentially faster with N than the noise. In particular, the noise per detector or per particle needs to be less than about 14%. In the absence of noise, detector efficiencies of around $1/\sqrt{2} \approx 71\%$ are required. This bodes well for the feasibility of the detection process. The efficiency of field ionization detectors used in micromaser systems is currently around 40% [39]. Improving both the efficiency of collection of electrons from ionized Rydberg states and the discrimination between Rydberg states prior to ionization is the subject of ongoing

research [45], and we are confident that the necessary detector efficiencies are attainable.

5. Conclusion

We have proposed two schemes for demonstrating exponential violations of Mermin's inequality in very different atomic systems. Besides their significance in tests of quantum mechanics versus local realism, the schemes we have proposed could be important tools in unambiguously creating and identifying genuine *N*-body entanglement in atomic systems as well as studying how decoherence affects them. The experimental techniques required, while challenging, are not far from what can currently be achieved in the laboratory.

References

[1] Bell J S 1964 *Physics* **1** 195–200
[2] Bell J S 1966 *Rev. Mod. Phys.* **38** 447–52
[3] Mermin N D 1990 *Phys. Rev. Lett.* **65** 1838–40
[4] Belinskiĭ A V and Klyshko D N 1993 *Phys.—Usp.* **36** 653–93
[5] Gisin N 1998 *Phys. Lett.* A **246** 1–6
[6] Werner R F and Wolf M M 2001 *Phys. Rev.* A **64** 032112
[7] Scarani V and Gisin N 2001 *Phys. Rev. Lett.* **87** 117901
[8] Seevinck M and Uffink J 2001 *Phys. Rev.* A **65** 012107
[9] Tóth G, Gühne O, Seevinck M and Uffink J 2005 *Phys. Rev.* A **72** 014101
[10] Yu S, Chen Z B, Pan J W and Zhang Y D 2003 *Phys. Rev. Lett.* **90** 080401
[11] Chen Y A, Yang T, Zhang A N, Zhao Z, Cabello A and Pan J W 2006 *Phys. Rev. Lett.* **97** 170408–1
[12] Rauschenbeutel A, Nogues G, Osnaghi S, Bertet P, Brune M, Raimond J M and Haroche S 2000 *Science* **288** 2024–8
[13] Monroe C *et al* 2000 *Nature* **404** 256–9
[14] Lü X Y, Si L G, Hao X Y and Yang X 2009 *Phys. Rev.* A **79** 052330
[15] Lü X Y, Song P J, Liu J B and Yang X 2009 *Opt. Express* **17** 14298–311
[16] Roos C F, Riebe M, Haffner H, Hansel W, Benhelm J, Lancaster G P T, Becher C, Schmidt-Kaler F and Blatt R 2004 *Science* **304** 1478–80
[17] Shimizu A and Morimae T 2005 *Phys. Rev. Lett.* **95** 090401
[18] Zou X B, Kim J and Lee H W 2001 *Phys. Rev.* A **63** 065801
[19] Gerry C and Campos R 2001 *Phys. Rev.* A **64** 063814
[20] Lee H, Kok P, Cerf N and Dowling J 2002 *Phys. Rev.* A **65** 030101
[21] Jacobson J, Björk G, Chuang I and Yamamoto Y 1995 *Phys. Rev. Lett.* **74** 4835–8
[22] Pan J W, Bouwmeester D, Daniell M, Weinfurter H and Zeilinger A 2000 *Nature* **403** 515–9
[23] Mitchell M W, Lundeen J S and Steinberg A M 2004 *Nature* **429** 161–4
[24] Leibfried D *et al* 2005 *Nature* **438** 639–42
[25] Dunningham J A and Burnett K 2001 *J. Mod. Opt.* **48** 1837–53
[26] Dunningham J and Burnett K 2004 *Phys. Rev.* A **70** 033601
[27] Cornish S L, Claussen N R, Roberts J L, Cornell E A and Wieman C E 2000 *Phys. Rev. Lett.* **85** 1795–8
[28] Greiner M, Mandel O, Esslinger T, Hänsch T W and Bloch I 2002 *Nature* **415** 39–44
[29] Denschlag J *et al* 2000 *Science* **287** 97–101
[30] Kim T, Ha Y, Shin J, Kim H, Park G, Kim K, Noh T G and Hong C 1999 *Phys. Rev.* A **60** 708–11
[31] Peil S, Porto J, Tolra B, Obrecht J, King B, Subbotin M, Rolston S and Phillips W 2003 *Phys. Rev.* A **67** 051603
[32] Li T C, Kelkar H, Medellin D and Raizen M G 2008 *Opt. Express* **16** 5465–70
[33] Sherson J F, Weitenberg C, Endres M, Cheneau M, Bloch I and Kuhr S 2010 *Nature* **467** 68–72
[34] Brune M, Hagley E, Dreyer J, Maître X, Maali A, Wunderlich C, Raimond J and Haroche S 1996 *Phys. Rev. Lett.* **77** 4887–90
[35] Sanguinetti B, Majeed H O, Jones M L and Varcoe B T H 2009 *J. Phys. B: At. Mol. Opt. Phys.* **42** 165004
[36] Zheng S B and Guo G C 2000 *Phys. Rev. Lett.* **85** 2392–5
[37] Osnaghi S, Bertet P, Auffeves A, Maioli P, Brune M, Raimond J and Haroche S 2001 *Phys. Rev. Lett.* **87** 037902
[38] Brattke S, Varcoe B and Walther H 2001 *Phys. Rev. Lett.* **86** 3534–7
[39] Englert B G, Löffler M, Benson O, Varcoe B, Weidinger M and Walther H 1998 *Fortschr. Phys.* **46** 897–926
[40] Blythe P J and Varcoe B T H 2006 *New J. Phys.* **8** 231
[41] Ryabtsev I I, Tretyakov D B and Beterov I I 2003 *J. Phys. B: At. Mol. Opt. Phys.* **36** 297–306
[42] Davydkin V A, Ovsyannikov V D and Zon B A 1993 *Laser Phys.* **3** 449–61 (http://www.maik.ru/full/lasphys/93/2/lasphys2_93p449full.pdf)
[43] Gallagher T F 1988 *Rep. Prog. Phys.* **51** 143–88
[44] Braunstein S and Mann A 1993 *Phys. Rev.* A **47** R2427–30
[45] Jones M L, Sanguinetti B, Majeed H O and Varcoe B T H 2010 *Appl. Soft Comput.* at press (doi: 10.1016/j.asoc.2010.07.005)(arXiv:0909.3217)